Production Engineering (2022) 16:503–512
https://doi.org/10.1007/s11740-021-01092-w

PRODUCTION PROCESS

Process design of a novel combination of peel grinding and deep rolling

Berend Denkena[1] · **Alexander Kroedel**[1] · **Tobias Gartzke**[1]

Received: 9 July 2021 / Accepted: 22 November 2021 / Published online: 4 December 2021

Abstract
Grinding is mostly considered as a finishing operation by which a high surface quality is achieved. An increase in productivity is therefore limited by maintained surface properties such as the roughness or tensile residual stresses. Thus, a roughing operation is inevitable followed by a finishing operation, while both operations are separated, leading to larger cycle times and process costs. In this paper, a novel process combination is investigated in which the roughing is done by grinding and the finishing operation by deep rolling within one tool setup. In this way, both processes are conducted parallel within the primary processing time. The objective of this study is the knowledge of the characteristics of this process combination with regard to the workpiece surface integrity. Therefore, shafts are ground in peel grinding with varying grinding wheel types and process parameters and subsequently machined with deep rolling. The process combination is evaluated with regard to the process forces and the resulting surface properties. In addition, experiments using the process combination were conducted in order to investigate the transferability of the results towards the process combination. By this approach, it was found that the surface roughness was reduced up to 80% by deep rolling showing the potential of the process combination.

Keywords Grinding · Deep rolling · Process combination · Topography

1 Introduction

The product quality in grinding is determined by surface properties such as the roughness or the residual stresses. An increase in productivity by e.g. the feed rate leads to a decreased surface quality in both, roughness and residual stresses. Therefore, the grinding process is further developed in order to reduce the process load and thus increase the surface quality. Common approaches are the structuring [1, 2] of grinding wheels as well as the change in grain or bond of the grinding wheel [3]. However, previous studies proofed that additional, subsequent processes such as the forming process deep rolling process can improve the surface quality [4, 5]. This process leads to a decreased roughness and an increase in compressive residual stresses, which is considered as a higher surface quality [6, 7].

Since additional processes lead to an increase in primary processing time, various authors investigated process combinations of machining and rolling processes that enable a simultaneous processing. Klocke developed a machine tool, which combines turning, grinding and deep rolling operations in one machine [8]. In this way, the roughing and finishing of hardened shafts is performed in one setup. This setup includes four cross tables with two grinding spindles, one deep rolling tool and a turret. Thus, the different tools engage at individual operation parameters but parallel in terms of the primary processing time. However, as the processing forces are relatively high and the engagement positions of the tools vary, deflections and subsequent geometrical deviations are a major challenge to the process combination.

In later studies, geometrical combined processes were developed. Maiß as well as Kuhlemann investigated the influence of a combination of hard turning and deep rolling on the surface quality [9, 10]. The roller ball in these works is mounted closely behind the turning insert in circumferential direction. Thus, the heat of the turning process can be used in the forming process, leading to increased compressive residual stresses in higher depth [10].

✉ Tobias Gartzke
gartzke@ifw.uni-hannover.de

[1] Institute of Production Engineering and Machine Tools (IFW), Leibniz University Hannover, An der Universität 2, 30823 Garbsen, Germany

A first approach to a combined tool setup for grinding and deep rolling was conducted by Charfeddine et al. They mounted a deep rolling tool in axial direction next to a CBN grinding wheel on the wheel enclosure [11]. Throughout this study, it was possible to achieve compressive residual stresses in depth of more than 2 mm. However, this setup leads to a high unidirectional load on the shaft due to the selection of one deep rolling tool.

Former studies showed the potential of a process combination of grinding and deep rolling but also the threat of unidirectional forces. Hence, a novel process combination is developed within this study. The tool setup uses two deep rolling tools, which are positioned relatively to the grinding wheel on the counter side. This setup aims on the reduction of tensions in the shaft and bearing forces, in which way the threat of deflections is reduced. Throughout this work, the individual process forces of the single processes as well as the shaft surface properties when combining grinding and deep rolling are investigated. This delivers a technological basis for the process combination.

2 Materials and methods

In order to examine dependencies between the single processes, the grinding and the deep rolling process are conducted mainly in a serial procedure. The experimental grinding operations were carried out on a Schaudt CR41 cylindrical grinding machine with Castrol Variocut G 600 as coolant lubricant (CL). Therefore, each shaft was ground with constant process condition and divided in areas for a variation of deep rolling conditions. The clamping in this machine is conducted between centres. The deep rolling process is conducted on a NTX1000 turn-mill centre from DMG Mori AG with a single deep rolling tool and emulsion as a hydraulic medium, as it is the common coolant in this machine tool. The hydraulic medium leaks technically at the ball interface, lubricating the interface between the ball and the shaft. The change in machine tool is necessary due to the relatively high deep rolling forces and the use of a single deep rolling tool in this part of the investigation. The clamping in this machine is realised by a chuck and a tailstock.

The grinding operation was conducted with seven different tool specifications in order to cover a wide range of industrial application. The range of tools consists of conventional sintered corundum (SC) as well as the super abrasive grain type cubic boron nitride (CBN). This is done with regard to increase the transferability of the approach into the industry. The specifications are shown in Table 1.

The machined shafts are in case of the CBN grinding wheels hardened 100Cr6 (hardness = 60 HRC) with a diameter of $d_w = 60$ mm and a length of $l_w = 300$ mm. In case of the conventional grinding wheels, shafts of soft normalised 16MnCr5 are machined, while the geometrical properties were kept constant.

The grinding process is peel grinding (Fig. 1), by which relatively high material removal rates are achieved [3, 12]. The high material removal rates result of an angled grinding wheel surface by which the total radial infeed a_e is reduced to an effective infeed $a_{e,eff}$. Such grinding wheels feature a roughing zone with an angle of $\alpha = 12°$ and a cylindrical finishing zone parallel to the workpiece contour.

The used cutting parameters are shown in Table 2. The cutting speed v_c is lower for the conventional grinding wheels due to the lower thermal conductivity of corundum in relation to CBN. The radial depth of $a_e = 100$ µm is comparably low for peel grinding but chosen with regard to the industrial common approach of near net shape semi-finished parts. The speed ratio of 70 represents the industrial standard for roughing processes and was also applied within the deep rolling process. The used process parameters of the deep

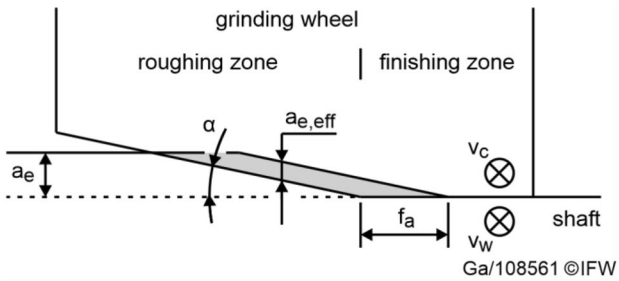

Fig. 1 Grinding process with relevant cutting parameters

Table 1 Used grinding wheel specifications

Abbreviation	Grain type	Grain size	Bonding type
B601	CBN	B601	Electroplated
B426	CBN	B426	Electroplated
B251	CBN	B251	Electroplated
B181	CBN	B181	Vitrified
B126	CBN	B126	Vitrified
SC60	Sintered corundum	F60	Vitrified
SC100	Sintered corundum	F100	Vitrified

Table 2 Used cutting parameters for the grinding process

Factor	Values
Cutting speed v_c (CBN)	100 m/s
Cutting speed v_c (SC)	50 m/s
Axial feed f_a	0.3/1.0/1.7 mm
Speed ratio q	70
Radial depth of cut a_e	100 µm

rolling process are listed in Table 3. This speed ratio causes a relatively low rolling speed for common deep rolling processes [13]. However, this was chosen, as the deep rolling process represents an addition to the grinding process. The axial feed was kept consistent in both, the grinding and the deep rolling process, in order to represent the later process combination. The deep rolling tools feature a cemented tungsten carbide roller ball.

Subsequently, the deep rolling tool was designed and implemented into the grinding machine. This part of investigation focuses the surface generation, as this is crucial in terms of transferability. The detailed investigation of the process combination is objective to later studies. In this part of the investigation, the novel deep rolling tool was used as shown in Fig. 2. The design of the deep rolling tool was published prior to this study in [14]. The deep rolling tool features swivels beneath the two modular deep rolling units, which enable a positioning of the tool towards the shaft. In addition, by means of the hydraulic stroke and a displacement from the centre it is possible to adjust the position of engagement of the deep rolling ball with the shaft. The position is described by the effective inclination angle θ and is used to achieve a force equilibrium of the applied machining forces on the shaft. Within this part of the investigation the hydraulic medium was the same oil CL as within the grinding process.

The measurement equipment in this investigation consists of a scanning electron microscope (SEM) Zeiss EVO 60 XVP (tungsten cathode), which is used for investigations on the generated surface on a microscopic level. The residual stresses were measured by X-Ray diffractometry with a GE XRD 3003 TT (beam: Cr Kα 30 kV, 35 mA). The surface roughness was determined with a perthometer Mahr Concept Roughness. For a deeper analysis, the surface was measured with a confocal white light microscope nanofocus µSurf. The grinding forces were measured by integrated piezoelectric force sensors. Regarding the test procedure, the grinding wheels with vitrified bond are dressed prior to each investigation, with an overlapping ratio $U_d = 4$ and a dressing depth of cut $a_{ed} = 5$ µm for 20 times. The galvanic plated grinding wheels were also dressed, even though they feature a single grinding layer. This was done in order to reduce a negative impact of protruding grains on the surface roughness. Accordingly, the dressing was conducted with the same dressing parameters as before but for 4 times. The dressing tool was a CVD-Diamond form roll with a width of 1 mm.

Table 3 Varied process setting values for the deep rolling process within the serial investigation mode

Factor	Values
Deep rolling tool	HG6/ HG13
Ball diameter d_k	6/13 mm
Pressure p_w	25/35/40/45 MPa
Axial feed f_a	0.3/1.0/ 1.7 mm
Rolling speed v_w	42/84.5 m/min

3 Results and discussion

3.1 Process forces

The process forces in grinding are essential to the design of the deep rolling tool. With known force values, it is possible to position the deep rolling contact point in relation to the shaft in order to minimise the resulting forces on the shaft. Subsequently, the bearing forces of the shaft are reduced,

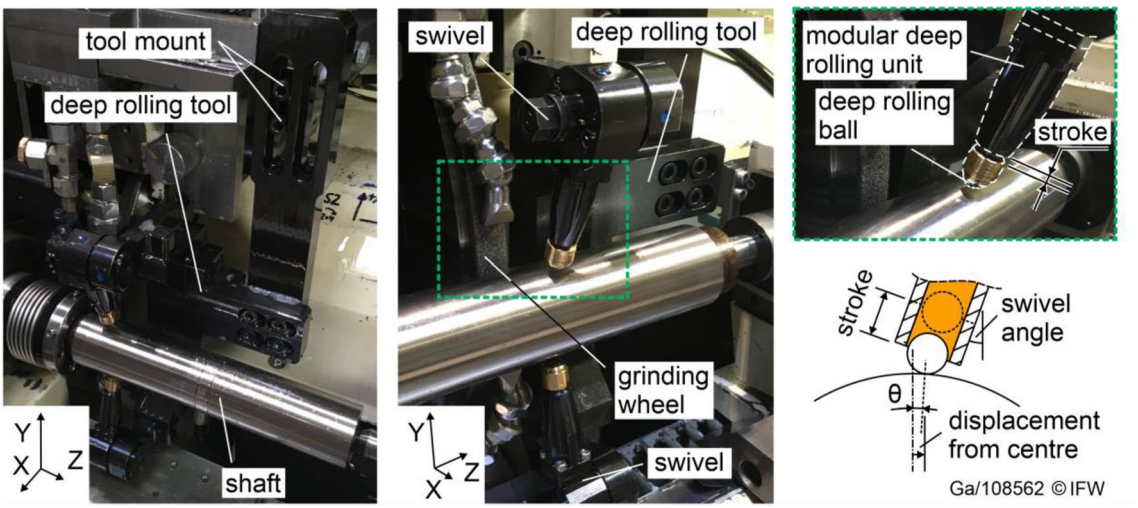

Fig. 2 Experimental setup of the grinding process and of the combined grinding and deep rolling process

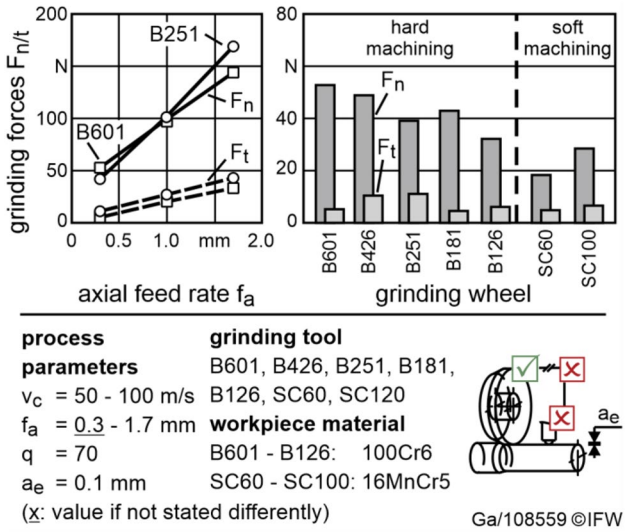

Fig. 3 Influence of the grinding process on the resulting grinding forces

which is essential as the shafts are clamped between centres. Moreover, the resulting deflection is reduced.

The results on the grinding forces show an incline with increasing feed rate as expected from the literature (Fig. 3) [15]. This behaviour was consistent for all grinding wheels and can be explained by the higher material removal rate with higher feed rate. The increase in grain size leads to relatively higher normal forces but smaller tangential forces when machining with low feed rate. As this equals a higher grinding force ratio, the high grain size B601 shows relatively more friction, which is explained by a reduced cutting angle for constant grain sizes in combination with low chip thicknesses. However, if the feed rate increases, the higher grain size caused a lower increase in normal forces and thus a lower grinding force ratio, as Fig. 3 illustrates on an example. The vitrified bonded CBN grinding wheels show lower grinding force ratios compared to galvanic plated CBN. However, the change in bond causes a change in grain distribution which limits the direct comparison of these tools. I.e. the galvanic plated CBN tools features a single grinding layer with higher grain protrusion. The process forces of the SC grinding wheels are remarkably low in relation to the CBN grinding tools. However, this is due to the workpiece material and its hardening state. The soft 16MnCr5 causes lower forces compared to the hardened 100Cr6. With regard to the novel process combination, the results on the grinding forces show that the grinding forces are mainly dependent on the feed rate. In order to achieve a force equilibrium between grinding and deep rolling forces, the deep rolling forces need to be adapted to the expected grinding forces.

The normal process force in deep rolling is calculated analytically, as the process force depends on the hydraulic conditions. Thus, the deep rolling force results of the pressure p_w and the intersection area of the roller ball with the diameter d_k. Additionally, a factor η describes the efficiency coefficient of the compressor system. The efficiency coefficient was determined by Denkena et al. to η = 0.79 for the tools of this study [13]. An increase in both, the ball diameter and rolling pressure leads to an increase of the deep rolling normal force as shown in Eq. (1).

$$F_{n,w} = \eta \cdot p_w \cdot \pi \cdot {d_k}^2 \cdot \frac{1}{4} \tag{1}$$

With known grinding force values F_n and the calculated deep rolling normal forces $F_{n,w}$ it is possible to calculated an inclination angle θ, for which a force equilibrium results Eq. (2). Tangential forces are neglected in this approach, as they are comparably little and as they equal a momentum that is absorbed by the workpiece spindle.

$$0 = \vec{F}_{n,w1} + \vec{F}_{n,w2} + \vec{F}_n \tag{2}$$

Equation (3) expresses $F_{n,w}$ in direction and orthogonal to F_n. In addition, the algebraic signs are adapted to the direction as shown in Fig. 4 below.

$$0 = F_{n,w1} \cdot (\sin(\theta) - \cos(\theta)) + F_{n,w2} \cdot (\sin(\theta) + \cos(\theta)) - F_n \tag{3}$$

As both deep rolling forces are equal ($F_{n,w1} = F_{n,w2} = F_{n,w}$), Eq. (3) can be reduced and rearranged to Eq. (4). With a further repositioning the inclination angle is calculated Eq. (5).

$$F_n = 2 \cdot F_{n,w} \cdot \sin(\theta) \tag{4}$$

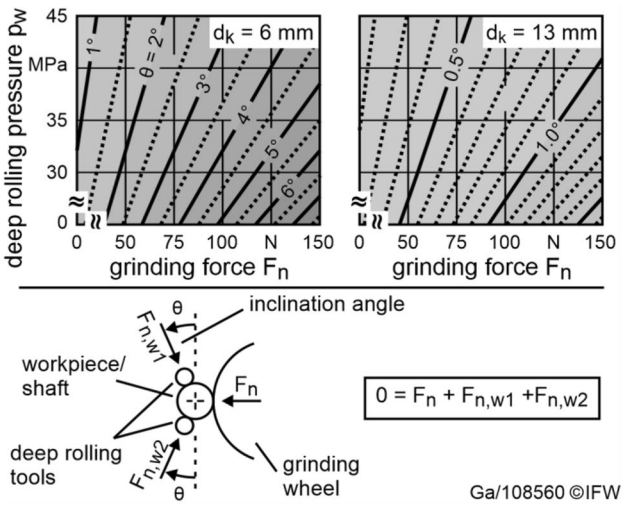

Fig. 4 Calculated inclination angle for varied grinding normal forces F_n and deep rolling pressures p_w

$$\theta = \arcsin\left(\frac{F_n}{2 \cdot F_{n,w}}\right) \tag{5}$$

Figure 4 shows the resulting inclination angle for a variation in grinding force F_n and in deep rolling pressure p_w. The expressed charts are used to set an inclination angle for a chosen grinding wheel and process feed rate within the following simultaneous machining process. The relatively small values of θ are due to the small values of F_n, which are caused by the small infeed of $a_e = 0.1$ mm for peel grinding processes. The designed tool is capable of a maximal inclination angle of $\theta_{max} = 35.7°$ for ideal positioning with $d_k = 13$ mm and $\theta_{max} = 31.6°$ for $d_k = 6$ mm. As the actual inclination angle is beneath 8° (Fig. 4) the tool design is capable to use both deep rolling ball diameters as well as all grinding wheel specifications and feed rates. In a further study at the IFW under similar conditions but an infeed of $a_e = 0.5$ mm, grinding normal forces were determined up to > 600 N [3]. With the deep rolling pressure range of this study, inclination angles of θ = 3.7°–6.6° (for $d_k = 13$ mm) and θ = 17.4°–32.5° (for $d_k = 6$ mm) result, which is still capable for the deep rolling tool. An increase in infeed equals a further potential to increase the overall process productivity. Furthermore, it is possible by these results to adjust the inclination angle in order to minimise the resulting processing force on the shaft.

3.2 Workpiece topography

The results on the surface roughness after the grinding process show an increase with increasing feed rate that can be explained by a reduced overlap of finishing zone paths of the grinding wheel. This is shown as a representative result in Fig. 5. According to the state of the art, it is expected that a decreasing grain size leads to a decreased surface roughness [15]. This effect was observed within one category of grinding wheel type only to a minor extend, with the exception of the relatively low roughness of grain size B426. The low level of roughness as well as the variation is explained by the dressing procedure, by which single protruding grains are levelled. In pre-test before dressing, surface roughness of Rz > 40 µm were examined. In case of the conventional grinding wheels, an untypical increase is observed. The higher roughness in case of SC100 was caused by clogging on the grinding wheel topography. Therefore, the roughness is mainly depended on the used axial feed rate. This incline in roughness reveals the potential for the process combination, by which the surface roughness is maintained at higher feed rates.

The results on the surface roughness after the deep rolling process show a decreasing roughness with increasing ball diameter and increasing rolling pressure up to 71%. Figure 6 illustrates these results on the example of the highest

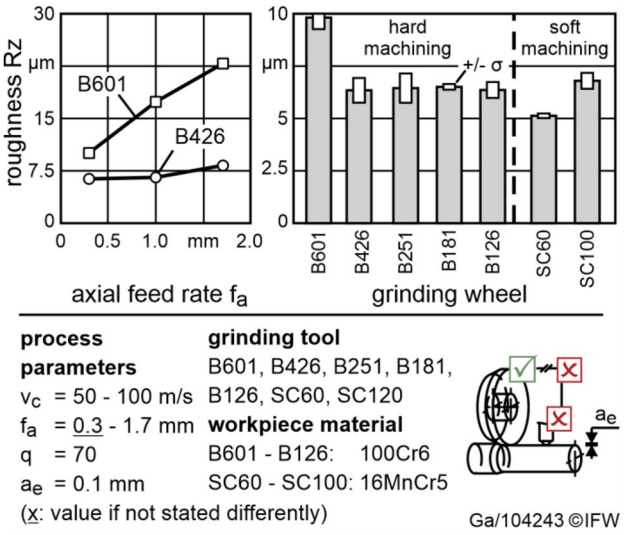

Fig. 5 Influence of the grinding process on the resulting surface roughness

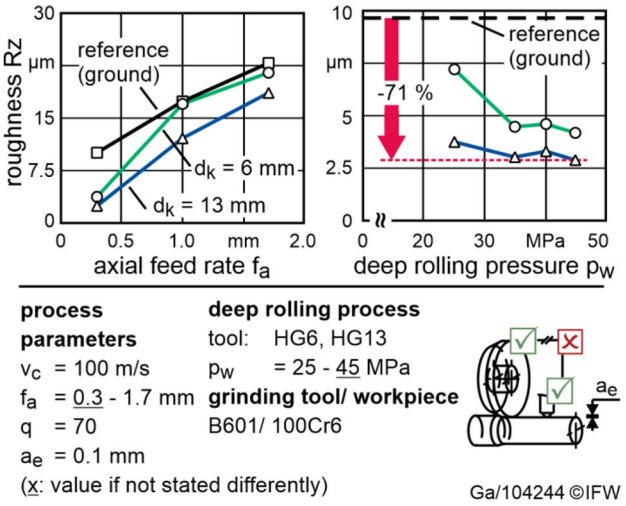

Fig. 6 Influence of the deep rolling process parameters on the resulting surface roughness

roughness after grinding, which resulted from the grinding wheel B601. The resulting roughness can be explained by the Hertzian contact conditions. According to Hertz, the contact width a_{pw} can be calculated by Eq. (6) [16].

$$a_{pw} = \sqrt[3]{\frac{1.5 \cdot (1 - \nu^2) \cdot F_{n,w} \cdot d_k}{2 \cdot E}} \tag{6}$$

Herein, ν is the combined Poisson's ratio and E the combined Young's modulus. They can be calculated by means of Eqs. (7) and (8) with the individual Young's moduli $E_{1/2}$ and Poisson ratios $\nu_{1/2}$ [17].

$$\frac{2}{E} = \left(\frac{1}{E_1} + \frac{1}{E_2}\right) \tag{7}$$

$$\frac{2 \cdot \nu}{E} = \left(\frac{\nu_1}{E_1} + \frac{\nu_2}{E_2}\right) \tag{8}$$

Therefore, an increase in deep rolling force as well as in ball diameter lead to an increase in contact width a_{pw}. A higher contact width however leads to a higher overlap of deep rolling paths, when maintaining the axial feed rate. With the process parameters of this study, the contact width is calculated for $d_k = 6$ mm in a range of $a_{pw} = 0.215$ mm ($p_w = 25$ MPa) to $a_{pw} = 0.261$ mm ($p_w = 45$ MPa). The range in contact width for $d_k = 13$ mm is $a_{pw} = 0.473$ mm ($p_w = 25$ MPa) to $a_{pw} = 0.575$ mm ($p_w = 45$ MPa). For this calculation the Young's modulus was set to $E = 210$ GPa for 100Cr6 and to $E = 600$ GPa for cemented tungsten carbide. The Poisson ratio was $\nu = 0.3$ (100Cr6) and $\nu = 0.21$ (cemented tungsten carbide).

The experimental results show that in case of an axial feed rate of $f_a = 0.3$ mm the increase in a_{pw} of + 120% by means of an increase in d_k does not correspond to an equally high effect on the surface roughness reduction. This can be explained by the overlap of deep rolling paths, which is negative for all $d_k = 6$ mm cases, however just slightly in case of $f_a = 0.3$ mm. The axial distance between two paths is with $a_{pw} = 0.261$ mm only 39 µm. The overlap is only in case of $d_k = 13$ mm and a feed rate of $f_a = 0.3$ mm positive. Accordingly, this negative overlap explains the decreasing effect of the deep rolling process on the roughness reduction with increasing axial feed rate. The decline in influence of the deep rolling process with increasing feed rate limits the achievable raise in productivity.

The surface roughness after deep rolling shows a strong dependence on the surface after grinding. In case of all CBN grinding wheels, a reduction in roughness of more than 70% was achieved for $f_a = 0.3$ mm (Fig. 7). The lower effect in case of the conventional grinding wheels is caused by the change in material. Due to the lower hardness, the shape of the roller ball was projected on the surface. This prompted in combination with a highly negative overlap an intense rise in roughness up to Rz = 65.8 µm ($f_a = 1.7$ mm; $d_k = 13$ mm; $p_w = 40$ MPa).

In order to generate a comprehensive understanding about the influence of the deep rolling process on the resulting surface of ground shafts, the resulting topography was investigated in more detail. Therefore, material contact area curves, SEM measurements and intersections of the shafts were evaluated for the grinding tool B601, as this tool shows the highest surface roughness. As Fig. 8 shows, deep rolling caused a compression of the entire profile but mainly on the heights, as illustrated on the maximum peak height. The related average reduced peak height Rpk was reduced from 0.9 to 0.3 µm.

The SEM measurements of the surface after the grinding process reveal burrs that can be explained by the material removal mechanism of ploughing (Fig. 9). These burrs were than clinched onto the surface by the following deep rolling process. In addition to the SEM measurements, microscopic pictures reveal that burrs and chips with remaining cohesion appear on all ground shafts. Therefore, this effect is not limited to a specific type of grinding wheel within this study. However, without specified application demands of the shaft, the generated surface does not represent a process limit to the process combination.

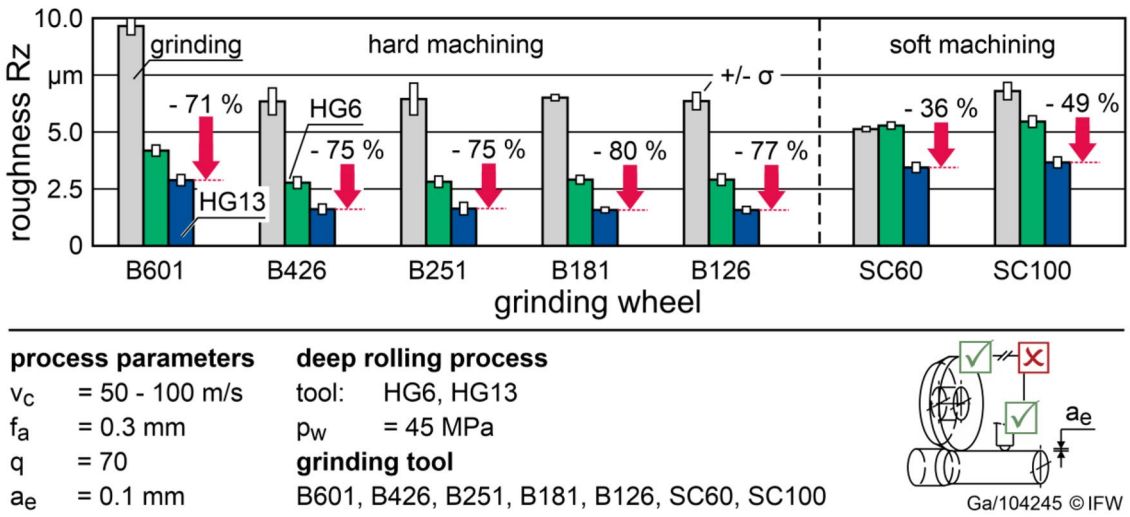

Fig. 7 Influence of the grinding wheel on the surface roughness after the deep rolling process

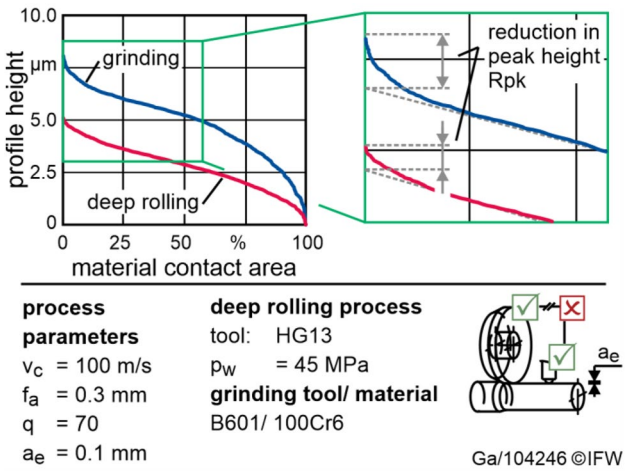

Fig. 8 Influence of deep rolling on the resulting surface shape

3.3 Residual stresses

The residual stresses were measured on the shafts that have been ground with the coarsest grinding wheel B601. The measurement results on the surface after grinding show that the residual stress values are mostly compressive (Fig. 10). Only in case of $f_a = 1.7$ mm a tensile stress value is observed, which represents a thermal induced damage. As expected from the state of the art, the deep rolling process leads to a shift of the residual stress towards higher compressive stress values. The coherence that negative overlaps prompt a decrease of the effect of the deep rolling process did not occur in this case. This can be explained by measurement spot size within the X-Ray diffractometry. With 2–4 mm this is significantly higher than the applied feed rate f_a. Subsequently, macroscopic changes in residual stresses are measured. The further analysis show a higher effect with increasing deep rolling pressure. The increased deep rolling force and the subsequent increased Hertzian pressure in the shaft surface under processing cause this effect. Additionally, the stress value in axial direction σ_a is higher compared to the circumferential direction σ_{ci} at both stages after grinding and after deep rolling. This can be explained by the processing direction. In both cases the tools engage in the circumferential direction with a subsequent friction that leads to tensile stress shares [18]. On the other side, both processes show a high lateral contact pressure with subsequent lateral material flow, i.e. ploughing. From these results it can be seen that an increase in feed rate, i.e. productivity, causes a shift of the residual

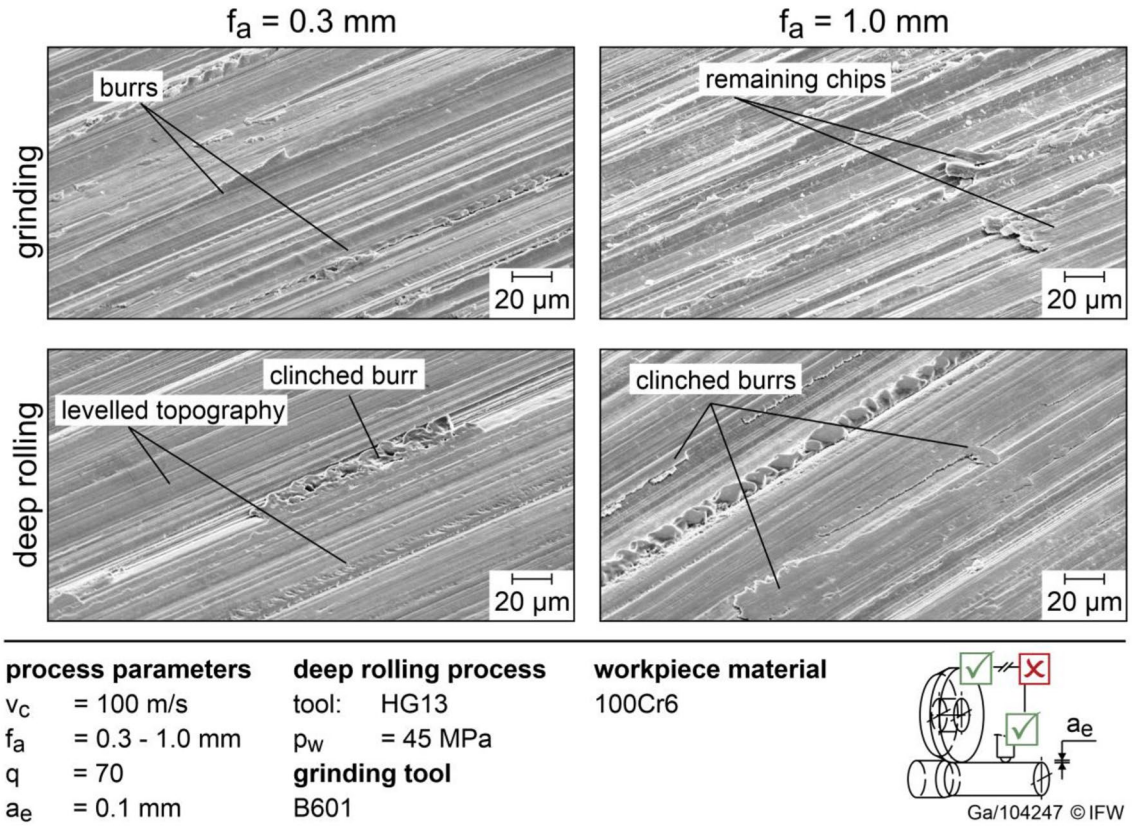

Fig. 9 Results of SEM measurements on the influence of the process step on the shaft topography

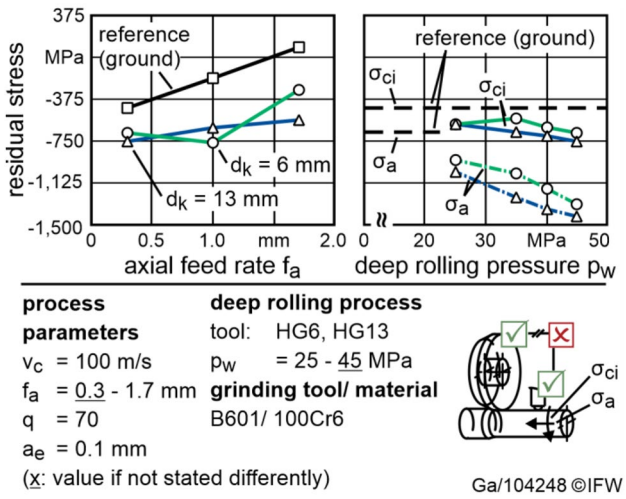

Fig. 10 Influence of deep rolling on the residual stress of the surfaces

stresses towards tensile stresses, which are considered as a process limit. The deep rolling process can compensate this raise in residual stress value, so that the feed rate can be raised, while maintaining the residual stress level. This, however, is limited by the negative overlap, by which parts of the shaft are not processed by deep rolling. This causes inconsistencies within the surface of the shaft. Due to the small infeed value of $a_e = 100$ µm, primarily compressive residual stresses resulted after grinding, which is why the surface roughness is considered as the predominant process limit within this study.

3.4 Simultaneous processing of grinding and deep rolling

Within the second experimental part of this study, the designed tool combination is implemented into the grinding machine. In order to determine the transferability of the established knowledge on surface generation to the process combination, the shaft topography is investigated after machining by means of the process combination. As shown in Fig. 11 the topography shows a macroscopic groove with a pitch equal to the feed. However, from a frequency analysis it can be seen that two engagement paths can be detected, as the spectrograph shows a secondary peak at a wavelength of $0.5 \cdot f_a$. When filtering the surface profile with a high pass filter with a cut-off of $\lambda_g < 0.5 \cdot f_a$, the engagement paths can be examined regarding depth and lateral distance. From the results, the profile can be described by a major groove with increased depth and a secondary groove with reduced depth. As the deep rolling tools engage under constant force load, the variation in groove depth is due to a change in deformation behaviour. From the geometrical process procedure, one of both deep rolling balls is leading. The second deep rolling ball is following partially within the groove of the first ball. For the explanation of this change in indention height two contrary explanatory approaches are likely. The first approach is that the leading ball causes a lower deformation capability of the workpiece, as it can be seen from the results on the residual stresses (Fig. 10). Thus, the secondary engagement depth is lower. On contrary, the second explanatory approach is that the secondary engagement prompts a deeper groove, as the respective material is processed twice,

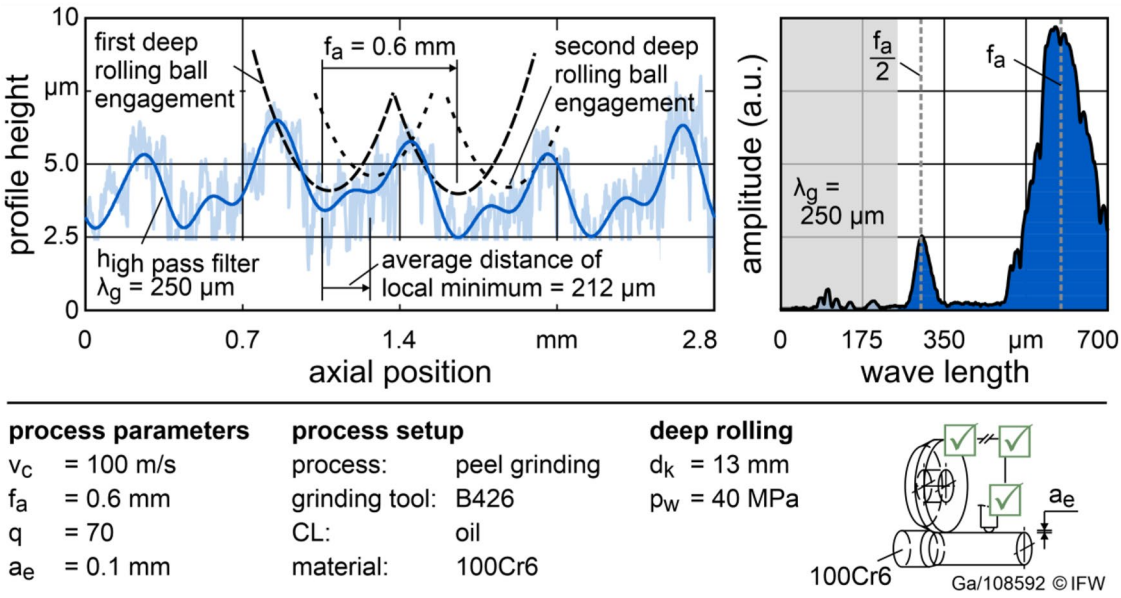

Fig. 11 Resulting surface profile after machining by means of the combined grinding and deep rolling process

i.e. with a positive overlap. Hence, the determination of the according mechanisms should be investigated in further studies.

Next to the height of the grooves, the lateral, axial distance between the grooves can be considered. This distance differs in the results from the half of the axial feed. The investigation of the cause is also objective to ongoing work. However, two main influencing factors affect the position of the groove. Firstly, the deep rolling balls feature a floating bearing. Thus, the following ball is forced to run within the leading groove. Secondly, the tolerance of the axial installation position causes a change in ideal engagement position.

These results demonstrate the transferability of the established technological basis for the process combination of peel grinding and deep rolling. The topography analysis also shows that the doubling of the deep rolling ball does not lead to two similar deep rolling paths. The existence of two similar grooves, however, is crucial for an additional increase in productivity by means of doubling the number of deep rolling balls.

4 Conclusion and outlook

Throughout this study, the technological basis for the process design of a novel combination of peel grinding and deep rolling was established. Therefore, shafts were ground with a variation of grinding tool type and process parameters. The measured forces are mainly $F_n < 150$ N, for which relatively low inclination angles of the deep rolling tools result. A low inclination angle is of importance to the tool design in order to enable a force equilibrium of process forces while featuring a passive mounting of the deep rolling tool and a movement of the tool setup towards the shaft. From the resulting surface roughness, it was outlined that the process combination is beneficial for a low feed rate due to a positive overlapping ratio. In this way, the roughness was reduced by up to 80%. The resulting topography can be described by clinched peak heights such as burrs, which was identified by SEM.

Furthermore, the transferability of the established data to the novel process combination was investigated. Therefore the novel combined tool setup was used to grind and deep roll a shaft simultaneously. Beside the change in procedure, the number of deep rolling balls was doubled in order to pursue a force equilibrium. From the subsequent results on the generated shaft topography, it was possible to achieve a proof of concept by which the transferability of the established data is indicated. However, it was also possible to detect two engagement paths, which differ in depth and axial position. Thus, the ideal potential doubling in feed rate, i.e. productivity, by doubling the number of deep rolling tools is limited by the actual generated surface. The influencing mechanisms on the position and shape of the deep rolling paths as well as the application behaviour of the novel process combination is subject to further studies. Herein, a major focus is on the force equilibrium as well as on the change in shaft topography under varying process parameters. In addition, the change from emulsion to oil as CL and subsequently as hydraulic medium leads to a fire risk, which is also to be investigated.

Acknowledgements The authors would like to thank the Federal Ministry for Economic Affairs and Energy (BMWi) Germany for their organizational and financial support within the project "Development of a combined process consisting of grinding and deep rolling for a productive machining rotationally symmetric workpieces" with the funding number "IGF 20433 N".

Funding Open Access funding enabled and organized by Projekt DEAL.

References

1. Denkena B, Krödel A, Gartzke T (2019) Process design of the patterning process of profile grinding wheels. Proc CIRP 86:126–132. https://doi.org/10.1016/j.procir.2020.01.011
2. Uhlmann E, Hochschild L (2013) Tool optimization for high speed grinding. Prod Eng Res Dev 7:185–193. https://doi.org/10.1007/s11740-013-0447-5
3. Denkena B, Krödel A, Wilckens M (2021) High performance peel grinding of steel shafts using coarse electroplated CBN grinding wheels. Prod Eng Res Dev. https://doi.org/10.1007/s11740-021-01047-1
4. Hettig M, Meyer D (2020) Sequential multistage deep rolling under varied contact conditions. Proc CIRP 87:291–296. https://doi.org/10.1016/j.procir.2020.02.027
5. Meyer D, Brinksmeier E, Hoffmann F (2011) Surface hardening by cryogenic deep rolling. Proc Eng 19:258–263. https://doi.org/10.1016/j.proeng.2011.11.109
6. Dzierwa A, Markopoulos AP (2019) Influence of ball-burnishing process on surface topography parameters and tribological properties of hardened steel. Machines 7(1):1–13. https://doi.org/10.3390/machines7010011
7. Abrão M, Denkena B, Köhler J, Breidenstein B, Mörke T (2014) The influence of deep rolling on the surface integrity of AISI 1060 high carbon steel. Proc CIRP 13:31–36. https://doi.org/10.1016/j.procir.2014.04.006
8. Klocke F (2006) Flexible Hochleistungs-Hart-End-Bearbeitung (HHFlex). Final report, BMBF 02 PD 2270

9. Maiß O, Denkena B, Grove T (2016) Hybrid machining of roller bearing inner rings by hard turning and deep rolling. J Mater Process Technol 230:211–216. https://doi.org/10.1016/j.jmatprotec.2015.11.029
10. Kuhlemann P, Denkena B, Grove T (2021) Hybrid soft machining of AISI 1045 by turn-rolling and its advantages. CIRP J Manuf Sci Technol 32:196–204. https://doi.org/10.1016/j.cirpj.2020.08.008
11. Charfeddine Y, Youssef S, Sghaier S, Sghaier J, Hamdi H (2020) Study of the simultaneous grinding/ball-burnishing of AISI 4140 based on finite element simulations and experiments. Int J Mech Sci 192:106097. https://doi.org/10.1016/j.ijmecsci.2020.106097
12. Rausch S, Biermann D (2012) High-performance surface peel grinding on conventional surface grinding machines. Proc CIRP 1:669–670. https://doi.org/10.1016/j.procir.2012.05.020
13. Denkena B, Grove T, Breidenstein B, Abrão M, Meyer K (2018) Correlation between process load and deep rolling induced residual stress profiles. Proc CIRP 78:161–165. https://doi.org/10.1016/j.procir.2018.09.063
14. Denkena B, Krödel A, Gartzke T (2020) Schleifwalzen—hybride Bearbeitung aus Schleifen und Walzen. Werkstatt + Betrieb 6, p 18
15. Tönshoff HK, Peters J, Inasaki I, Paul T (1992) Modelling and simulation of grinding processes. Ann CIRP 41(2):677–688
16. Böge A, Böge G, Böge W (2015) Festigkeitslehre. In: Böge A, Böge W (eds) Handbuch Maschinenbau. Springer, New York
17. Kalker JJ (2000) Rolling contact phenomena—linear elasticity. In: Jacobsen B, Kalker JJ (eds) Rolling contact phenomena. Springer, Wien
18. Broszeit E, Zwirlein O, Adelmann J (1982) Werkstoffanstrengung im Hertzschen Kontakt—Einfluß von Reibung und Eigenspannungen. Zeitschr Werkstofftechn 13:423–429